Polar Histograms of Curvature for Quantifying Skeletal Joint Shape and Congruence

Eni Halilaj
Center for Biomedical Engineering
and School of Engineering,
Brown University,
Providence, RI 02912

David H. Laidlaw
Department of Computer Science,
Brown University,
Providence, RI 02912

Douglas C. Moore
Department of Orthopaedics,
The Warren Alpert Medical School
of Brown University and Rhode Island Hospital,
Providence, RI 02903

Joseph J. Crisco[1]
Department of Orthopaedics,
The Warren Alpert Medical School
of Brown University and Rhode Island Hospital,
Providence, RI 02903
e-mail: joseph_crisco@brown.edu

The effect of articular joint shape and congruence on kinematics, contact stress, and the natural progression of joint disease continues to be a topic of interest in the orthopedic biomechanics literature. Currently, the most widely used metrics of assessing skeletal joint shape and congruence are based on average principal curvatures across the articular surfaces. Here we propose a method for comparing articular joint shape and quantifying joint congruence based on three-dimensional (3D) histograms of curvature—shape descriptors that preserve spatial information. Illustrated by experimental results from the trapeziometacarpal joint, this method could help unveil the interrelations between joint shape and function and provide much needed insight for the high incidence of osteoarthritis (OA)—a mechanically mediated disease whose onset has been hypothesized to be precipitated by joint incongruity. [DOI: 10.1115/1.4027938]

1 Introduction

In the skeletal system, form and function are closely related. Studies in evolutionary biology have continually sought to discern the morphological differences that have led to functional differences among taxa [1,2]. Similarly, differences in articular shape and congruence within species may grant insight into pathological processes such as OA [3–7]—a progressive disease of articular cartilage and bone [8–11] whose underlying pathoetiology is believed to be mediated by altered joint mechanics [12–14].

Quantitative analyses of articular morphology that span beyond simple morphometric measurements are necessary to identify subtle differences that may play a significant role in joint biomechanics. The most widely used metrics for describing articular joint shape are the average principal (minimum, k_{min}, and maximum, k_{max}) curvatures, the Gaussian curvature (k_{gauss}), the mean curvature (k_{mean}), and the average root-mean-square curvature (k_{rms}) (Appendix A) [1,15–17]. While these metrics provide important information on the overall curvature of a surface, they may not discriminate between differently shaped surfaces because they do not preserve spatial information. An alternative method for describing joint shape is based on fitting circles or ellipsoids to the articular surfaces [18], but this method is not extendable to joints with concave and convex portions (e.g., saddle joints). Statistical shape models (SSMs) have also been used to describe whole bone shape [19–21] and to identify drastic changes in bony morphology that occur with severe pathology [21,22]. The feasibility of SSMs and circle- or ellipsoid-fitting methods in identifying subtle anatomical differences in articular geometry, however, has not been demonstrated.

Joint congruence—described as the agreement between mating articular surfaces—is related to the ability of a joint to distribute stresses and is highly depended on joint posture. Based on Hertzian contact theory, joint congruence has been expressed in terms of the curvature of two opposing surfaces at the point of contact (Appendix B) [15,23]. Various implementations of this theory have been proposed, such as the utilization of average principal curvatures across the whole articular areas, average principal curvatures from the estimated areas of contact, and principal curvatures from the centroids of the contact areas [15,24]. Average curvature metrics based on the whole articular surface areas do not incorporate joint posture information, which is important in the assessment of congruence. Utilization of the principal curvatures from the contact areas is an improved alternative, but the in vivo determination of contact areas in small joints remains challenging with current limitations in imaging resolution.

Given that the similarity between two complex geometries cannot be assessed effectively with scalar metrics, which do not consider spatial correspondence between the surfaces under comparison, we propose to represent the articular surfaces with polar histograms of curvature—compact 3D shape representations that preserve spatial information [25]. In addition to using the histograms to compare the articular surface of a given bone across cohorts of subjects (Sec. 2), we propose a method that integrates the histogram representations from the two mating surfaces of a joint into a posture-dependent congruence measure (Sec. 3). To illustrate the efficacy of the proposed methods, we present results from the saddle-shaped trapeziometacarpal joint, located at the base of the thumb (Sec. 4).

2 Articular Shape Analysis

The methods described here are intended for 3D models, such as nonuniform rational b-spline (NURBS) surfaces, polygon meshes, or point-clouds of articular joints. The analysis is performed on the articular facets, after they have been selected from the whole bone models. In Secs. 2.1 and 2.2, we describe how the articular surface of a bone is represented by a shape descriptor, which in our case is a polar histogram of curvature (Sec. 2.1), and how shape descriptors are compared across subjects to determine group differences in the articular morphology of a given bone (Sec. 2.2).

2.1 Polar Histograms of Curvature as Articular Shape Descriptors. Given subject-specific 3D articular surface models, two key concepts must be considered in order to enable efficient and meaningful shape comparison: model abstraction and alignment. Model abstraction entails defining a structured representation—a fixed-dimensional feature vector or a shape descriptor of the anatomy—that contains predefined shape information, e.g., local curvature. Alignment of the objects to be compared ensures that there is anatomically meaningful correspondence among the shape descriptors of different subjects. In this section, we describe a shape descriptor for articular joint surfaces, which through a

[1]Corresponding author.

Manuscript received February 3, 2014; final manuscript received June 23, 2014; accepted manuscript posted July 2, 2014; published online July 21, 2014. Assoc. Editor: Kristen Billiar.

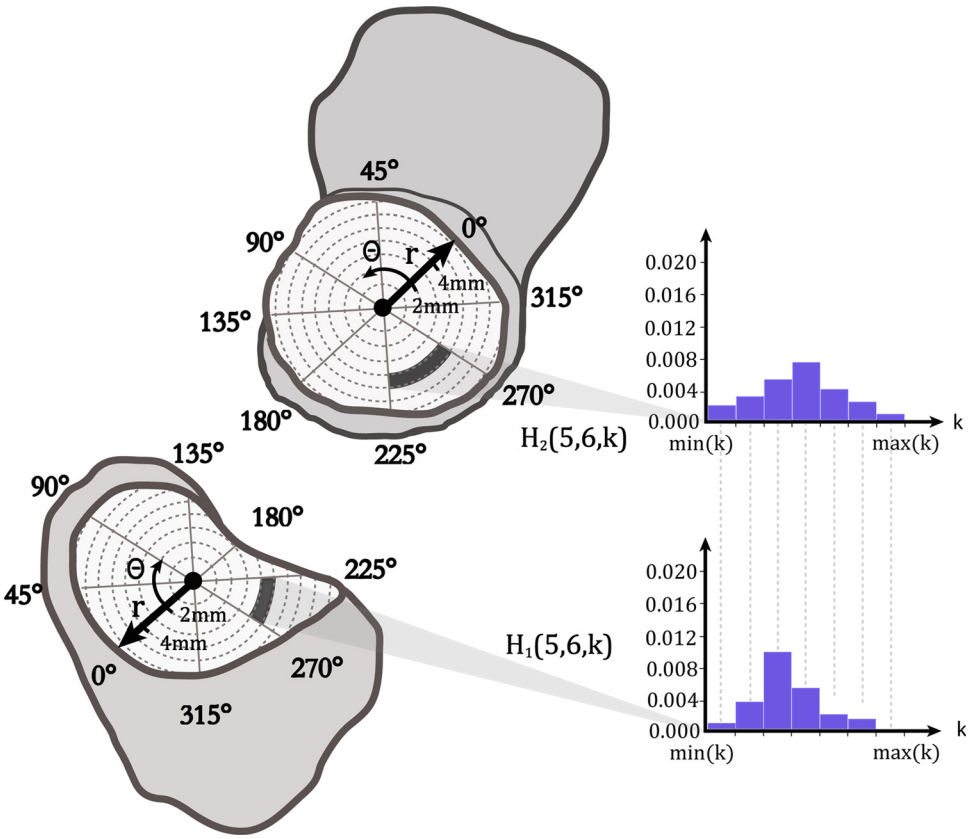

Fig. 1 Polar coordinate systems on the mating articular surfaces of a joint, illustrating the dimensions of the 3D histograms: the radial coordinate or the distance from the pole (*r*), the angular coordinate or the angle from the polar axis (θ), and curvature (*k*)

series of preprocessing steps is rendered invariant to translation, rotation, and scaling, thereby facilitating intersubject comparison.

We propose that subject-specific articular geometry be represented by a 3D polar histogram [25] of curvature. Since curvature is not invariant to size, we suggest that the articular surface models be isotropically scaled to remove the effect of size, but to preserve shape. The articular surfaces of anatomical joints typically contain a distinct inflection point, which is used as the pole of the coordinate system. With the exception of ball-and-socket type joints, where it may be more appropriate to use 2D shell histograms [25], most articular joints, such as condyloid, hinge, and saddle joints, are also characterized by directions of maximum and minimum curvature, one of which is used as the polar axis (Fig. 1). The distance from the pole and the angle from the polar axis, r and θ, respectively, are then two of the dimensions of the histogram, whereas curvature is the third. In short, while a 1D histogram of curvatures across the articular surface requires binning of the range of curvature values, a 3D polar histogram requires binning of the r range (0 to r_{max})—shells—and the θ range (0–2π)—sectors, as well as the curvature range (0 to k_{max}). Since the articular surface is 3D, but the polar coordinate system is 2D, the coordinate system is projected as orthogonal to the surface normal of the inflection point. Principal curvatures across the articular surface may be computed directly on the meshed surface [26] or on an analytic surface fitted to the vertices [15]. To ensure that the histogram optimally represents the structure of the underlying data, we suggest that the histogram bin size be optimized in accordance with the data by using previously proposed rules [27].

2.2 Intersubject Comparison With Support Vector Machines (SVM). To identify group differences in a given sample, we propose using the SVM learning algorithm, which has been shown to perform well in the classification of high-dimensional data [28]. Briefly, the SVM algorithm is a nonprobabilistic classifier which, given n-dimensional data points from x groups, aims to determine the optimal separation of the n-dimensional space such that each data point is furthest apart from the separation boundary. When a linear classifier is chosen, the separation boundary is a line for 2D data, a plane for 3D data, and a hyperplane for 4D + data. Depending on the complexity of the data, kernel functions may be used instead of linear classifiers. Testing for group differences can be achieved with a Student's t test of the signed distance between each histogram and the optimal separation hyperplane. The method proposed here differs from a statistical test of the average principal curvatures in that the articular shapes are represented and compared in a high-dimensional space to determine the optimal separation hyperplane. The subsequent use of the signed distance from the hyperplane is equivalent to data-dimensionality reduction.

3 Joint Congruence

Congruence is determined here by computing a modified Bhattacharyya distance [29] between the polar histograms of the mating articular surfaces. The Bhattacharyya distance is well-suited for determining the dissimilarity between two discrete probability distributions—e.g., two histograms H_1 and H_2—in a way that meaningfully represents the dissimilarity of the represented 3D objects [30]

$$D_B(H_1, H_2) = -\ln\left(\sum_{x \in X} \sqrt{H_1(x) H_2(x)}\right) \quad (1)$$

This, however, is a metric that is based solely on geometry, while the congruence of a joint depends on both bone geometry and

physiological joint position. Therefore, we propose computing the histogram of one of the articular surfaces in the coordinate system of its mating articular surface and calling it a *dynamic histogram*, dH_2. The dissimilarity between H_1 and dH_2 is then computed at each position, and this serves as a position-dependent congruence measure. We further propose incorporating a linear weighting factor that is inversely proportional to the bone-to-bone distance for each bin-to-bin comparison. This weighting factor ensures that the parts of the mating articular-surface areas that are in closer physical proximity have a higher weight on the final congruence metric. First, the minimum bone-to-bone distance is computed for each point on the articular surfaces, creating a map of interbone distances. The distance map is simplified to mean distances for each physical bin ($r\ x\ \theta$), yielding a height field, h, of b^2 elements, which serves as a look-up table to assist in determining the weight of each bin-to-bin comparison. The simplification is implemented because the points within a bin may have different minimum bone-to-bone distances. In Fig. 1, for example, the bone-to-bone distance for the highlighted physical bins is represented by one mean value, h_{30}, because in each of the seven bins in $H_1(5,6,k)$, there are points with different bone-to-bone distances. The surface points are classified into each curvature range independently of their physical location within the highlighted physical bin. The weight, w_x, of each bin, with a mean bone-to-bone distance of h_x, is then

$$w_x = \frac{b^2}{hx * \sum_{y=1:b^2} \frac{1}{h_y}} \tag{2}$$

and positional joint congruence, pJC, is computed as follows:

$$p\mathrm{JC}(H_1, dH_2) = -\ln\left(\sum_{x\in X} w_x * \sqrt{H_1(x) * dH_2(x)}\right) \tag{3}$$

4 Implementation in the Thumb Carpometacarpal (CMC) Joint

The thumb CMC joint, located at the base of the thumb, is a saddle-shaped articulation that is often susceptible to OA. Morphological changes in the articular surface of the trapezium—the carpal bone in the joint—at advanced stages of the disease have been identified computationally and are detectible even observationally (Fig. 2). To our knowledge, potential differences between healthy subjects and patients in the early stages of the disease have not been reported in current literature. We analyzed the CMC joints (Fig. 3(*a*)) of 35 subjects with early stage CMC OA (Eaton Stage I/II) [31] and 35 age-matched healthy subjects to determine group differences in the articular shape of the trapezium (Sec. 4.1) and in the congruence of the joint across eight scanned positions (Sec. 4.2), with our methods and with the previously used metrics. Prior to enrollment in the study, the arthritic subjects were screened by a board-certified orthopedic surgeon to insure that they had one or more positive clinical signs and little or no radiographic evidence of CMC OA.

4.1 Articular Shape of the Trapezium. After receiving approval from our Institutional Review Board, computed tomography (CT) image volumes of the dominant wrists and thumbs of all the subjects were captured at a resolution of $0.3\,\mathrm{mm} \times 0.3\,\mathrm{mm} \times 0.625\,\mathrm{mm}$ or better. The bones in the CMC joint were segmented semi-automatically (Mimics, Leuven, Belgium) from the CT volumes and exported as 3D meshed surfaces (Fig. 3(*b*)). The trapezial bone models were isotropically scaled by $\sqrt[3]{(V_{\mathrm{avg}}/V_{\mathrm{s}})}$, where V_{s} is the subject-specific bone volume and V_{avg} is the average bone volume in a dataset of s subjects. The isotropic scaling of the bone models, which involves scaling of linear measures, i.e., the coordinates of the control points, can also be carried out with a surface-area-based factor, but since we found a direct correlation between the two factors ($R^2 = 0.97$; $p < 0.0001$), we proceeded to using the volume-based factor. The articular surfaces on the trapezium were manually selected by following the subchondral margins on the bone models (Fig. 3(*b*)). A fifth order polynomial surface was fitted to the vertices of the meshed articular surface (Fig. 3(*c*)) [15]. Principal curvature magnitudes and directions were then computed at 400 pts/mm^2 uniformly sampled across the fitted surface (Fig. 3(*d*)). The local inflection point on each surface was determined with a second partial derivative test (Appendix C) and the direction of maximum curvature for the surface was determined by computing a sum of the maximum curvature vector field. k_{min} and k_{max} histograms, as well as average k_{min} and k_{max}, were then determined for each subject. A histogram bin size of 7 was chosen for each of the three dimensions of the histogram.

An SVM with a linear classifier was used to find the optimal separation hyperplane between the histograms of the healthy and the early OA groups. A Student's t test of the signed distance from each histogram to the optimal hyperplane demonstrated a

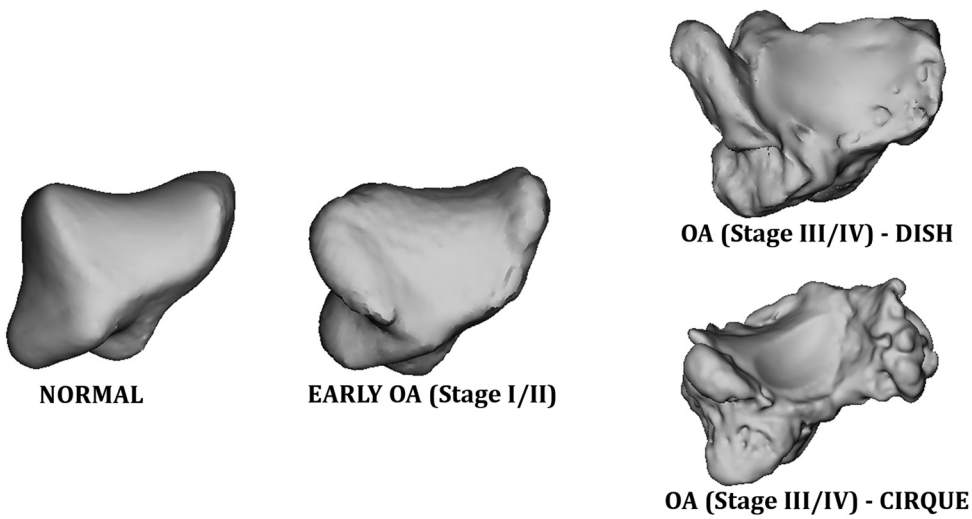

Fig. 2 Illustration of arthritic progressions in the trapezium, with 3D bone models extracted from CT scans of volunteers (normal, early OA) and excised trapezia of patients who underwent trapeziectomy (late stage OA)

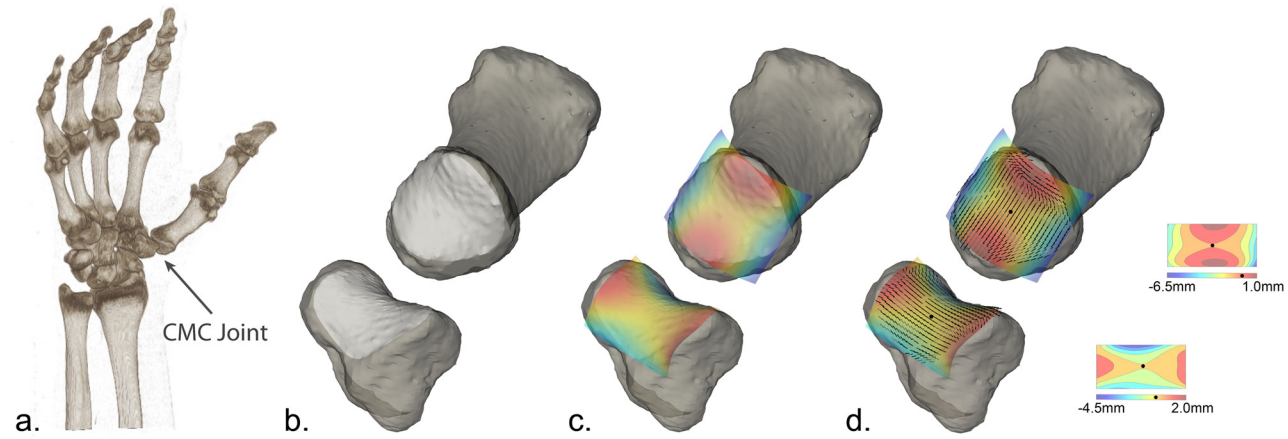

Fig. 3 (*a*) 3D bone models of a wrist and hand from a CT scan, (*b*) manually selected subchondral facets on the trapeziometacarpal joint, (*c*) the fifth order polynomial surfaces fitted to the facets, and (*d*) minimum curvature vector fields on the fitted surface ranging from 0 to 0.45 mm^{-1}, represented here at lower resolution, for visual purposes

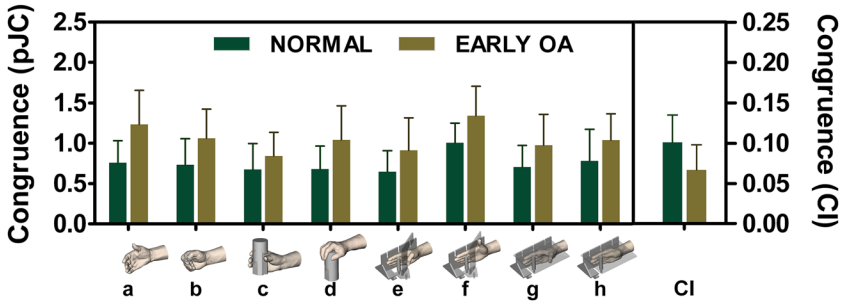

Fig. 4 The mean (±SD) position specific dissimilarity measure, *p*JC, in the normal and arthritic groups during (*a*) neutral, (*b*) key pinch, (*c*) jar grasp, (*d*) jar open, (*e*) extension, (*f*) flexion, (*g*) abduction, and (*h*) adduction position, as well as the previously used CI, where, for both *p*JC and CI, a higher value indicates lower congruence

significant difference between the articular shape of the trapezia of healthy subjects and the trapezia of patients with early stage OA ($p = 0.0079$ for k_{min} and $p = 0.0133$ for k_{max} histograms; Fig. 3). The significance level was set at 0.025 to account for multiple comparisons. The differences between the average principal curvatures of the articular surfaces in healthy trapezia and OA trapezia were not statistically significant (normal subjects: $k_{min} = -73 \pm 17\,m^{-1}$, $k_{max} = 120 \pm 20\,m^{-1}$; early OA subjects: $k_{min} = -85 \pm 26\,m^{-1}$, $k_{max} = 110 \pm 24\,m^{-1}$; Student's *t*-test results: $p_{min} = 0.578$, $p_{max} = 0.1053$).

4.2 Trapeziometacarpal Joint Congruence. All the participating subjects were scanned with their wrists and thumbs in a neutral position, during three functional tasks (key pinch, jar grasp, and jar open), and during four maximum thumb range-of-motion positions (extension, flexion, abduction, and adduction). Thumb posture was standardized with custom-designed polycarbonate jigs. During the functional tasks, subjects were scanned with their hand relaxed in the prescribed positions. 3D bone models were generated by segmenting the neutral position CT volume and articular facets were manually delineated on both the trapezium and metacarpal, as previously described. 3D kinematics of the trapezium and metacarpal from the neutral position to the remaining positions were determined with a markerless bone registration algorithm [32]. Joint congruence, *p*JC, for each thumb position was then computed from the k_{max} histogram of the trapezium and the k_{min} dynamic histogram of the metacarpal, since the directions of principal curvatures in the trapezium and metacarpal are offset by approximately 90 deg. The previously used congruence index (CI) was also computed for comparison [15].

A multivariate analysis of variance of the *p*JC across different joint postures revealed that the thumb CMC joints in subjects with early signs of OA are less congruent than in normal subjects (Fig. 4; the *p* values of the post hoc tests for pairwise comparisons were <0.0001, 0.0001, 0.0289, 0.0001, 0.0071, 0.0003, 0.0045, and 0.0083 for neutral, key pinch, jar grasp, jar open, extension, flexion, abduction, and adduction postures, respectively). In contrast, the CI was lower (better congruence) for the OA group than the healthy group ($p < 0.0001$; Fig. 4).

5 Discussion

We have described a method that enables the comparison of 3D articular joint surfaces across subjects and have defined a joint congruence measure that takes into account articular morphology and physiological position. With accompanying experiments, we demonstrated that the proposed methods: (1) can identify morphological changes that occur in the early stages of CMC OA, which previous average curvature metrics did not identify and (2) suggest that joints in the early stage of OA have decreased congruence, while, in contrast, the previously used CI suggests that arthritic joints have better congruence than healthy joints. Since better congruence is associated with higher mechanical stability, it is highly unlikely that arthritic joints have higher congruence than healthy joints from subjects of the same age. CI is based on morphology alone and does not account for positional information. The same research group that proposed the CI has demonstrated

that, contrary to what the CI indicates, better geometrical similarity between two mating articular surfaces does not always result in improved joint contact [33].

While offering several advantages in comparison to the previous metrics, the methods proposed here have limitations or characteristics that must be considered. First, our congruence measure compares the magnitude, but not the direction, of the principal curvatures of corresponding areas in the mating surfaces. The simplification of the principal directions of curvature of the mating surfaces to 90 deg is consistent with previous methods, but the advantage of the current implementation is that the comparison of magnitudes is position-dependent. Second, the purpose of implementing a weighting factor in the congruence measure is to amplify the contribution of curvature comparisons in areas that are in closer physical proximity. We chose a weighting factor that is linearly proportional to the bone-to-bone proximity, but other nonlinear functions may be more appropriate. We have not investigated the utility of other weighting factors. We found, however, that when no weighting factor is implemented, the dissimilarity measure yields no group differences. Third, the construction of polar histograms may be difficult to achieve in severely arthritic joints, where there may be irregular transformations in the articular surfaces. The current methods are intended for investigating subtler differences, rather than cases involving gross pathological change.

Exploring tools that are sensitive to fine variations in bony morphology will help evolutionary biologists and orthopedic biomechanists track natural variations in skeletal functional morphology that may relate to adaptation and, most importantly, disease. We recognize that there are other approaches for shape analysis that preserve spatial information that could yield desirable results, e.g., SSMs, spherical harmonics, and other feature-based descriptors [34]. These methods, however, have not been employed for articular surface comparison in current literature, and performing a comparative analysis is beyond the scope of this paper. Our purpose was to offer an alternate approach to the currently used average-curvature metrics for the shape analysis and congruence of articular joints and let the particular scientific questions and future experimental results dictate the utility of each method.

Acknowledgment

The authors would like to thank Dr. A.-P. C. Weiss, Dr. A. L. Ladd, A. Garcia, J. B. Schwartz, J. C. Tarrant, T. K. Patel, and B. Berg for their contributions to this work. This work was supported by NIH AR059185.

Nomenclature

CI = congruence index
H = mean curvature
K = Gaussian curvature
k_{max} = maximum curvature
k_{min} = minimum curvature
k^e_{max} = equivalent minimum curvature
k^e_{min} = equivalent maximum curvature
k_{rms} = root-mean-square curvature
α = the angle between the principal directions of curvature on the point of contact between the two articular surfaces

Appendix A: Principal Curvatures

The principal curvatures (minimum, k_{min}, and maximum, k_{max}) measure the minimum and maximum bending of a surface, $f(x, y)$, at a specific point [35]. They are related to the Gaussian curvature, K, and the mean curvature, H, as follows:

$$k_{max} = H + \sqrt{(H^2 - K)} \tag{A1}$$

$$k_{min} = H - \sqrt{(H^2 - K)} \tag{A2}$$

where

$$K = \frac{f_{xx}f_{yy} - f_{xy}^2}{(1 + f_x^2 + f_y^2)^2}$$

$$H = \frac{f_{xx} + f_{yy} + f_{xx}f_y^2 + f_{yy}f_x^2 - f_x f_y f_{xy}}{2(1 + f_x^2 + f_y^2)^{1.5}}$$

Previous studies have also employed the root-mean-square curvature as a measure of surface flatness [15]

$$k_{rms} = \sqrt{\frac{k_{min}^2 + k_{max}^2}{2}} \tag{A3}$$

Appendix B: Average Curvature-Based CI

The congruence of a joint depends on the curvature of the articulating surfaces at the point of contact; let us call these articulating surfaces S_1 and S_2, with the following principal curvatures at the point of contact: k_{max1}, k_{min1}, k_{max2}, and k_{max2}, respectively. To compute congruence, an "equivalent system" has been proposed, where the equivalent surface, S^e represents the difference between S_1 and S_2. Congruence can then be determined between a plane and S^e by using only the principal curvatures, k^e_{min} and k^e_{max}, of the equivalent surface, computed as follows:

$$k^e_{min} = D_1 + D_2 - \sqrt{A_1^2 + A_2^2 + 2A_1A_2\cos 2\alpha} \tag{B1}$$

$$k^e_{max} = D_1 + D_2 + \sqrt{A_1^2 + A_2^2 + 2A_1A_2\cos 2\alpha} \tag{B2}$$

where

$$D_1 = k_{min1} - k_{max1}$$
$$D_2 = k_{min2} - k_{max2}$$
$$A_1 = \frac{1}{2}(k_{min1} + k_{max1})$$
$$A_2 = \frac{1}{2}(k_{min2} - k_{max2})$$

Since determining the point of contact in a joint is not feasible in vivo, a simplification has been proposed by Ateshian et al., wherein the average curvatures of the whole surfaces are used instead of the principal curvatures at the point of contact [15]. After computing the equivalent curvatures as shown above, and assuming that α is 90 deg—since the principal curvatures between the two articulating surfaces on a saddle joint are approximately 90 deg apart—the CI is then computed as follows:

$$\text{CI} = \sqrt{\frac{(k^e_{min})^2 + (k^e_{max})^2}{2}} \tag{B3}$$

The idea is that if $S_1$and S_2 were perfectly congruent, then the equivalent surface S^e (the difference between them) would be a plane, where $k^e_{min} = k^e_{max} = 0 \overset{\text{yields}}{\rightarrow} \text{CI} = 0$.

Appendix C: Local Saddle Point

In a given surface, $f(x, y)$, a critical point, $f(a, b)$, determined as follows:

$$f_x(a,b) = f_y(a,b) = 0$$

is a saddle point if $\begin{vmatrix} f_{xx}(a,b) & f_{xy}(a,b) \\ f_{yx}(a,b) & f_{yy}(a,b) \end{vmatrix} < 0$ [36].

References

[1] Marzke, M. W., Tocheri, M. W., Steinberg, B., Femiani, J. D., Reece, S. P., Linscheid, R. L., Orr, C. M., and Marzke, R. F., 2010, "Comparative 3D Quantitative Analyses of Trapeziometacarpal Joint Surface Curvatures Among Living Catarrhines and Fossil Hominins," Am. J. Phys. Anthropol., **141**(1), pp. 38–51.

[2] Tocheri, M. W., Razdan, A., Williams, R. C., and Marzke, M. W., 2005, "A 3D Quantitative Comparison of Trapezium and Trapezoid Relative Articular and Nonarticular Surface Areas in Modern Humans and Great Apes," J. Hum. Evol., **49**(5), pp. 570–586.

[3] Williams, G. M., Chan, E. F., Temple-Wong, M. M., Bae, W. C., Masuda, K., Bugbee, W. D., and Sah, R. L., 2010, "Shape, Loading, and Motion in the Bioengineering Design, Fabrication, and Testing of Personalized Synovial Joints," J. Biomech., **43**(1), pp. 156–165.

[4] Beck, M., Kalhor, M., Leunig, M., and Ganz, R., 2005, "Hip Morphology Influences the Pattern of Damage to the Acetabular Cartilage Femoroacetabular Impingement as a Cause of Early Osteoarthritis of the Hip," J. Bone Joint Surg. Br., **87-B**(7), pp. 1012–1018.

[5] Colombo, V., Palla, S., and Gallo, L. M., 2008, "Temporomandibular Joint Loading Patterns Related to Joint Morphology: A Theoretical Study," Cells Tissues Organs, **187**(4), pp. 295–306.

[6] Daniel, M., Iglic, A., and Kralj-Iglic, V., 2005, "The Shape of Acetabular Cartilage Optimizes Hip Contact Stress Distribution," J. Anat., **207**(1), pp. 85–91.

[7] Noble, P. C., Kamaric, E., Sugano, N., Matsubara, M., Harada, Y., Ohzono, K., and Paravic, V., 2003, "Three-Dimensional Shape of the Dysplastic Femur: Implications for THR," Clin. Orthop., **417**, pp. 27–40.

[8] Smith, R. W., Egger, P., Coggon, D., Cawley, M. I., and Cooper, C., 1995, "Osteoarthritis of the Hip Joint and Acetabular Dysplasia in Women," Ann. Rheum. Dis., **54**(3), pp. 179–181.

[9] Felson, D. T., Zhang, Y., Hannan, M. T., Naimark, A., Weissman, B. N., Aliabadi, P., and Levy, D., 1995, "The Incidence and Natural History of Knee Osteoarthritis in the Elderly, the Framingham Osteoarthritis Study," Arthritis Rheum., **38**(10), pp. 1500–1505.

[10] Felson, D. T., and Zhang, Y., 1998, "An Update on the Epidemiology of Knee and Hip Osteoarthritis With a View to Prevention," Arthritis Rheum., **41**(8), pp. 1343–1355.

[11] Richette, P., Corvol, M., and Bardin, T., 2003, "Estrogens, Cartilage, and Osteoarthritis," Jt., Bone, Spine, **70**(4), pp. 257–262.

[12] Wilson, D. R., McWalter, E. J., and Johnston, J. D., 2008, "The Measurement of Joint Mechanics and Their Role in Osteoarthritis Genesis and Progression," Rheum. Clin. North Am., **34**(3), pp. 605–622.

[13] Hunter, D. J., and Wilson, D. R., 2009, "Imaging the Role of Biomechanics in Osteoarthritis," Rheum. Clin. North Am., **35**(3), pp. 465–483.

[14] Hunter, D. J., and Wilson, D. R., 2009, "Role of Alignment and Biomechanics in Osteoarthritis and Implications for Imaging," Radiol. Clin. North Am., **47**(4), pp. 553–566.

[15] Ateshian, G. A., Rosenwasser, M. P., and Mow, V. C., 1992, "Curvature Characteristics and Congruence of the Thumb Carpometacarpal Joint: Differences Between Female and Male Joints," J. Biomech., **25**(6), pp. 591–607.

[16] Hohe, J., Faber, S., Muehlbauer, R., Reiser, M., Englmeier, K. H., and Eckstein, F., 2002, "Three-Dimensional Analysis and Visualization of Regional MR Signal Intensity Distribution of Articular Cartilage," Med. Eng. Phys., **24**(3), pp. 219–227.

[17] Kwak, S. D., Colman, W. W., Ateshian, G. A., Grelsamer, R. P., Henry, J. H., and Mow, V. C., 1997, "Anatomy of the Human Patellofemoral Joint Articular Cartilage: Surface Curvature Analysis," J. Orthop. Res., **15**(3), pp. 468–472.

[18] Allaire, S., Jacq, J. J., Burdin, V., and Roux, C., 2007, "Ellipsoid-Constrained Robust Fitting of Quadrics With Application to the 3D Morphological Characterization of Articular Surfaces," Conf. Proc. IEEE Eng. Med. Biol. Soc., **2007**, pp. 5087–5090.

[19] Kozic, N., Weber, S., Büchler, P., Lutz, C., Reimers, N., González Ballester, M. A., and Reyes, M., 2010, "Optimisation of Orthopaedic Implant Design Using Statistical Shape Space Analysis Based on Level Sets," Med. Image Anal., **14**(3), pp. 265–275.

[20] Heimann, T., and Meinzer, H.-P., 2009, "Statistical Shape Models for 3D Medical Image Segmentation: A Review," Med. Image Anal., **13**(4), pp. 543–563.

[21] Bredbenner, T. L., Eliason, T. D., Potter, R. S., Mason, R. L., Havill, L. M., and Nicolella, D. P., 2010, "Statistical Shape Modeling Describes Variation in Tibia and Femur Surface Geometry Between Control and Incidence Groups From the Osteoarthritis Initiative Database," J. Biomech., **43**(9), pp. 1780–1786.

[22] Giessen, M., Raedt, S., Stilling, M., Hansen, T. B., Maas, M., Streekstra, G. J., Vliet, L. J., and Vos, F. M., 2011, "Localized Component Analysis for Arthritis Detection in the Trapeziometacarpal Joint," *Medical Image Computing and Computer-Assisted Intervention—MICCAI 2011*, G. Fichtinger, A. Martel, and T. Peters, eds., Springer, Berlin, Heidelberg, pp. 360–367.

[23] Lurie, A. I., 1964, *Three-Dimensional Problems of the Theory of Elasticity*, J. R. M. Radok, ed., Interscience, New York.

[24] Connolly, K. D., Ronsky, J. L., Westover, L. M., Küpper, J. C., and Frayne, R., 2009, "Analysis Techniques for Congruence of the Patellofemoral Joint," ASME J. Biomech. Eng., **131**(12), p. 124503.

[25] Ankerst, M., Kastenmüller, G., Kriegel, H.-P., and Seidl, T., "3D Shape Histograms for Similarity Search and Classification in Spatial Databases," *Advances in Spatial Databases*, R. H. Güting, D. Papadias, and F. Lochovsky, eds., Springer Berlin, Heidelberg, Berlin, Heidelberg, pp. 207–226.

[26] Taubin, G., 1995, "Estimating the Tensor of Curvature of a Surface From a Polyhedral Approximation," Proceedings of Fifth International Conference on Computer Vision, pp. 902–907.

[27] Maciejewski, R., 2011, "Data Representations, Transformations, and Statistics for Visual Reasoning," Synth. Lect. Vis., **2**(1), pp. 1–85.

[28] Vapnik, V. N., 1999, "An Overview of Statistical Learning Theory," IEEE Trans. Neural Network, **10**(5), pp. 988–999.

[29] Bhattacharyya, A., 1943, "On a Measure of Divergence Between Two Statistical Populations Defined by Their Probability Distributions," Bull. Calcutta Math. Soc., **35**, pp. 99–109.

[30] Cha, S.-H., 2007, "Comprehensive Survey on Distance/Similarity Measures Between Probability Density Functions," Int. J. Math. Model. Meth. Appl. Sci., **1**(4), pp. 300–307.

[31] Eaton, R. G., and Glickel, S. Z., 1987, "Trapeziometacarpal Osteoarthritis. Staging as a Rationale for Treatment," Hand Clin., **3**(4), pp. 455–471.

[32] Marai, G. E., Laidlaw, D. H., and Crisco, J. J., 2006, "Super-Resolution Registration Using Tissue-Classified Distance Fields," IEEE Trans. Med. Imaging, **25**(2), pp. 177–187.

[33] Xu, L., Strauch, R. J., Ateshian, G. A., Pawluk, R. J., Mow, V. C., and Rosenwasser, M. P., 1998, "Topography of the Osteoarthritic Thumb Carpometacarpal Joint and Its Variations With Regard to Gender, Age, Site, and Osteoarthritic Stage," J. Hand Surg., **23**(3), pp. 454–464.

[34] Bronstein, A. M., Bronstein, M. M., and Ovsjanikov, M., 2012, "Feature-Based Methods in 3D Shape Analysis," *3D Imaging, Analysis and Applications*, N. Pears, Y. Liu, and P. Bunting, eds., Springer, London, pp. 185–219.

[35] Banchoff, T. F., and Lovett, S. T., 2010, *Differential Geometry of Curves and Surfaces*, CRC Press, Boca Raton, FL.

[36] Stewart, J., 2011, *Multivariable Calculus*, Cengage Learning, Belmont, CA.